J. Chem. Sci. (2022) 134:43
https://doi.org/10.1007/s12039-022-02037-1

REGULAR ARTICLE

Selective detection of Cu^{2+} by benzothiazole-based colorimetric chemosensor: a DFT study

JAE SUNG HEO, BOEON SUH and CHEAL KIM*
Department of Fine Chem. and Renewable Energy Convergence, Seoul National Univ. of Sci. and Tech., Seoul 01811, Korea
E-mail: chealkim@seoultech.ac.kr

MS received 15 November 2021; revised 27 January 2022; accepted 27 January 2022

Abstract. An effectively selective colorimetric chemosensor **BTV** (2-methoxy-6-((E)-(((E)-3-methylbenzo[*d*]thiazol-2(3H)-ylidene)hydrazono)methyl)phenol) was synthesized for detecting Cu^{2+}. The **BTV** having benzothiazole group showed a bathochromic shift (150 nm) with an explicit color variation from colorless to pink toward Cu^{2+}. The **BTV** could detect Cu^{2+} down to 0.37 μM in solution. The binding ratio of **BTV** and Cu^{2+} was determined to be a 1:2 by Job plot and ESI-MS. Sensor **BTV** could distinctly sense Cu^{2+} without interference from other cations and distinguish it from diverse metal ions through the test strip. The sensing process of Cu^{2+} by **BTV** was presented by UV-visible titration, Job plot, ^{1}H NMR titration, DFT calculation, FT-IR and ESI-MS.

Keywords. Copper; Benzothiazole; Bathochromic shift; Test strip; DFT calculation.

1. Introduction

Copper, which is largely used in modern industry, has excellent erosion resistance, thermal conductivity, and electrical conductivity.[1–4] With these excellent properties, it is utilized in the manufacturing field of pipes, motors, and alloys.[5–7] However, excessive use of copper leads to various environmental pollutions in soil and ocean. Especially, it has triggered a critical effect on the soil associated with ecological safety, for example, bacterial tolerance to toxic metals and critical harm to land creatures.[8–15] Because of these reasons, the sensing of copper ions is essential in controlling its critical effect on the ecosystem.

There are several ways to detect copper, like inductively coupled plasma optical emission spectroscopy (ICP-OES),[16,17] flame atomic absorption spectroscopy (FAAS), and atomic absorption spectroscopy (AAS).[18] Although these methods have the advantage capable of determining low concentration with good accuracy, they have some problems like high cost, long analysis time, and sophisticated instruments.[19–22] By contrast, colorimetric techniques that the metal target ion can be aptly probed *via* the colorimetric variation have advantages such as low cost,[23] specificity, [24] simplicity,[25] and easy detection *via* naked-eye.[26] For these reasons, effective colorimetry chemosensors for probing copper are needed to be developed.

The number of the reported Cu^{2+} sensors showed their colorimetric characteristic, and they utilized several functional groups such as chalcone, rhodamine, coumarin, pyrazine, dansyl amide, naphthalimide, and so on.[27–33] Among them, benzothiazole moiety, known as a good chromophore and fluorophore, has excellent photostability and unique spectral properties.[34,35] Particularly, benzothiazole has sulfur in its structure, which has a great affinity to Ag^+, Cu^{2+}, and Hg^{2+}. Some sulfur-containing sensors were reported to sense these three metals.[36,37] To detect selectively only harder Cu^{2+} among them, we combined benzothiazole with vanillin moiety having hard oxygen atoms.[38]

Herein, we described a benzothiazole-based colorimetric sensor **BTV** for Cu^{2+}, which was synthesized by condensation of benzothiazole moiety and ortho

*For correspondence
Supplementary Information: The online version contains supplementary material available at https://doi.org/10.1007/s12039-022-02037-1.

Published online: 14 March 2022

vanillin. Compound **BTV** displayed a great bathochromic shift (150 nm) with an explicit color variation from colorless to pink toward Cu^{2+}. The utilization of **BTV** was greatly practical because test strips could be applied at a low concentration of copper ion. The detection mechanism of **BTV** to Cu^{2+} was demonstrated through UV-visible experiments, ^{1}H NMR titration, density functional theory (DFT) calculations, Fourier-transform infrared spectroscopy (FT-IR) and electrospray ionization mass spectrometry (ESI-MS).

2. Experimental

2.1 *Materials and equipment*

Chemicals were commercially provided. ^{1}H and ^{13}C NMR spectra were collected by using a Varian spectrometer. Elemental analysis for C, H, N, and S was performed with a Vario Mario MICRO Cube elemental analyzer. UV-visible and ESI-MS data were provided by a Perkin Elmer UV-visible spectrometer and an Acquity SQD quadrupole machine. FT-IR spectra were obtained with a Thermo Fisher Scientific Fourier Transform Infrared Spectrophotometer -2.

2.2 *Synthesis of BTV*

3-Methyl-2-benzothiazolinone-hydrazone hydrochloride (215.0 mg, 1 mmol) and *o*-vanillin (152.1 mg, 1 mmol) were dissolved in 5.0 mL methanol. The solution was stirred for 25 min at room temperature. The yellowish fine solid produced was filtered and rinsed with ether to give **BTV**. **BTV** dried at 70 °C in oven for 15 h (yield: 92%). ^{1}H NMR in dimethylsulfoxide-d_6 (DMSO-d_6): δ 10.81 (s, 1H), 8.62 (s, 1H), 7.69 (d, 1H), 7.36 (m, 2H), 7.13 (t, 2H), 7.01 (d, 1H), 6.86 (t, 1H), 3.80 (s, 3H), 3.62 (s, 3H). ^{13}C NMR data in DMSO-d_6: δ 165.3 (1C), 154.0 (1C), 147.8 (1C), 147.3 (1C), 140.8 (1C), 126.8 (1C), 122.5 (2C), 122.0 (1C), 121.7 (1C), 119.1 (2C), 113.9 (1C), 110.4 (1C), 55.9 (1C), 30.9 (1C). ESI-MS: (m/z) [**BTV** + H_2O + H^+]$^+$ calcd for $C_{16}H_{18}N_3O_3S^+$, 332.11; found, 331.93 (Figs. S1-S3). Elemental analysis: calcd (%) for $C_{16}H_{15}N_3O_2S$ (**BTV**): C, 61.32; H, 4.82; N, 13.41; S, 10.23; found (%): C, 61.41; H, 5.01; N, 13.85; S 10.21,

2.3 *UV-visible selectivity*

3.0 μL (5×10^{-3} M) of **BTV** (1.6 mg, 5×10^{-6} mol) dissolved in DMSO (1 mL) was put into 2.997 mL MeCN to make 5 μM. For metal-ion stocks, 1×10^{-4} mol of $Fe(NO_3)_3$, $Al(NO_3)_3$, $Ga(NO_3)_2$, $In(NO_3)_2$, $Cr(NO_3)_3$ KNO_3, $Fe(ClO_4)_2$, $Pb(NO_3)_2$, $Hg(NO_3)_2$, $Mg(NO_3)_2$, $AgNO_3$, $Cr(NO_3)_3$, $NaNO_3$, $Mn(NO_3)_2$, $Zn(NO_3)_2$, $Co(NO_3)_2$, $Cd(NO_3)_2$, $Cu(NO_3)_2$, $Ca(NO_3)_2$ and $Ni(NO_3)_2$ was dissolved in 5.0 mL acetonitrile (MeCN), respectively. 3.0 μL of each cation was put into **BTV**. UV-visible data were obtained after 8 sec.

2.4 *UV-visible titrations*

3.0 μL (5×10^{-3} M) of **BTV** (1.6 mg, 5×10^{-6} mol) dissolved in DMSO (1,000 μL) was put into 2.997 mL MeCN to afford 5 μM. $Cu(NO_3)_2$ (11.9 mg, 1×10^{-4} mol) was dissolved in 5.0 mL MeCN. 0.15, 0.3, 0.45, 0.6, 0.75, 0.9, 1.05, 1.2 and 1.35 μL of Cu^{2+} stock were added to each **BTV** (5 μM), respectively. UV-visible data were obtained after 8 sec.

2.5 *Job plot*

300 μL of **BTV** (1.6 mg, 5×10^{-6} mol) dissolved in DMSO (1,000 μL) was diluted in 29.7 mL MeCN to give 5×10^{-5} M. 300-2,700 μL of diluted **BTV** were delivered into each UV-visible cell. 75 μL of $Cu(NO_3)_2$ (11.9 mg, 1×10^{-4} mol) dissolved in MeCN (5 mL) was diluted to 29.925 mL MeCN to afford 5×10^{-5} M. 300-2,700 μL of the Cu^{2+} were delivered to UV-visible cells for making a total volume of 3 mL. UV-visible data were obtained after 8 sec.

2.6 *Inhibition tests*

BTV solution (5×10^{-6} M) and metal-ion stocks (20 mM) were prepared as mentioned in the selectivity section. 3.0 μL of each cation and Cu^{2+} was delivered to the **BTV** to provide 5 μM. UV-visible data were obtained after 8 sec.

2.7 *^{1}H NMR titration*

The two NMR glass tubes of **BTV** (5 mmol, 0.8 mg) dissolved in DMSO-d_6 (500 μL) were made. 0 and 2.0 equiv. of Cu^{2+} dissolved in 100 μL of dimethylformamide-d_7 (DMF-d_7) were delivered to NMR tubes of **BTV** and ^{1}H NMR data were gained after 30 sec.

2.8 *Test strips*

A filter paper was divided into several pieces. They were immersed in **BTV** (5 mM) in DMF and dried for 7 h. After the filter paper dried off, 0.25 mM of Cu^{2+} dissolved in MeCN was used to determine the lowest concentration of visible variation. The varied cations (Ga^{3+}, Zn^{2+}, Fe^{2+}, Fe^{3+}, Cd^{2+}, Cr^{3+}, Hg^{2+}, Co^{2+}, Mg^{2+}, Ni^{2+}, Ag^{+}, Ca^{2+}, Pb^{2+}, In^{3+}, K^{+}, Al^{3+}, Mn^{2+}, and Na^{+}, 0.25 mM) in MeCN were tested with the paper strips.

2.9 *Calculations for BTV and BTV-2·Cu^{2+}*

Calculations of **BTV** and **BTV**-2·Cu^{2+} were implemented with the Gaussian 16 program.[39] DFT calculations and B3LYP were applied for geometry optimization.[40,41] As the hybrid-correlation functional, 6-31G(d,p) was used for all atoms except copper ion and los alamos national laboratory 2 double zeta (LANL2DZ) was used for Cu^{2+} to apply effective core potential (ECP).[42–45] The imaginary frequencies of **BTV** and **BTV**-2·Cu^{2+} were not displayed, indicating local minima of the optimized structures. To consider solvent interaction with **BTV**, IEFPCM was applied in all calculations.[46] time-dependent (TD)-DFT calculations were conducted to determine possible UV-visible transition states by referring to the optimized structures of **BTV** and **BTV**-2·Cu^{2+}.

3. Results and Discussion

BTV was provided from the reaction of *o*-vanillin and 3-methyl-2-benzothiazolinone-hydrazone hydrochloride (Scheme 1).

BTV was verified by ESI-MS, ^{1}H, and ^{13}C NMR (Figures S1-S3, SI). The absorbance of **BTV** proportionally increased to the concentration increase of **BTV** in the UV region (Figure S4, SI). The sensing capability and process of **BTV** toward Cu^{2+} were studied by several analytical tools like UV-visible titration, Job plot, calculations, and ESI-MS analysis.

3.1 *Colorimetry examinations of BTV toward Cu^{2+}*

The detecting capability of **BTV** was tested with varied cations like Fe^{3+}, Cd^{2+}, Cr^{3+}, Hg^{2+}, Cu^{2+}, Ga^{3+}, Zn^{2+}, Fe^{2+}, Co^{2+}, Mg^{2+}, Ni^{2+}, Ag^{+}, Ca^{2+}, Pb^{2+}, In^{3+}, K^{+}, Al^{3+}, Mn^{2+} and Na^{+} in varied organic solutions (DMF, DMSO, MeOH and MeCN) and aqueous solution. Cu^{2+} induced spectral and color variations from colorless to pink only in MeCN, whereas no color changes were shown with other cations (Figure 1).

Cd^{2+} and Fe^{3+} exhibited a little increase in absorption around 410 nm, but no color variation was observed with the naked eye. The outcomes confirmed that **BTV** can be utilized as a greatly selective colorimetry chemosensor for Cu^{2+}. To figure out the interaction process of **BTV** and Cu^{2+}, UV-visible titration was conducted (Figure 2).

The reaction of **BTV** with various concentrations of Cu^{2+} showed the two-step change (Figure 2(a)). In the first step (Figure 2(b)), the absorbance band around 357 nm was continuously decreased, and that of 507 nm increased with a bathochromic shift of 150 nm. A clean isosbestic point at 380 nm showed up. In the second stage (Figure 2(c)), the absorbance band around 377 nm was decreased and a clean isosbestic point showed up at 400 nm. These results signified that **BTV** combined with two Cu^{2+} ions *via* the two-step binding process. The detection limit of **BTV** to Cu^{2+} ($3\sigma/k$) was determined as 0.37 μM (Figure 3), where σ is the standard deviation of the blank solution and k is the slope of the calibration plot.

Particularly, the value is the lowest among benzothiazole-based colorimetry chemosensors for sensing Cu^{2+} (Table S1, SI).[47–50]

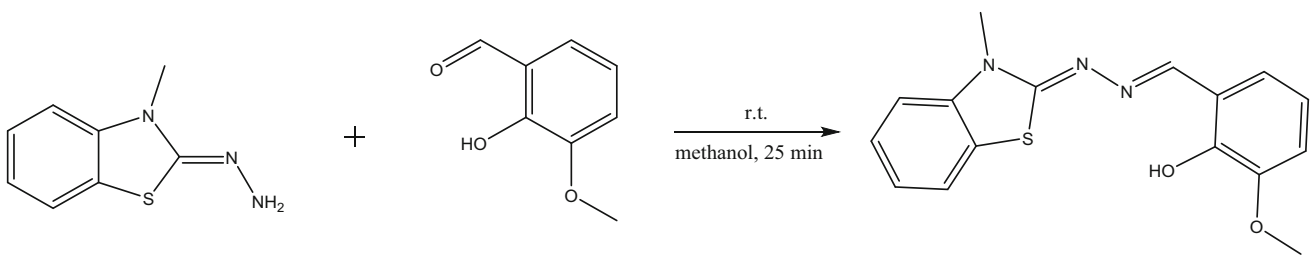

Scheme 1. Synthesis of **BTV**.

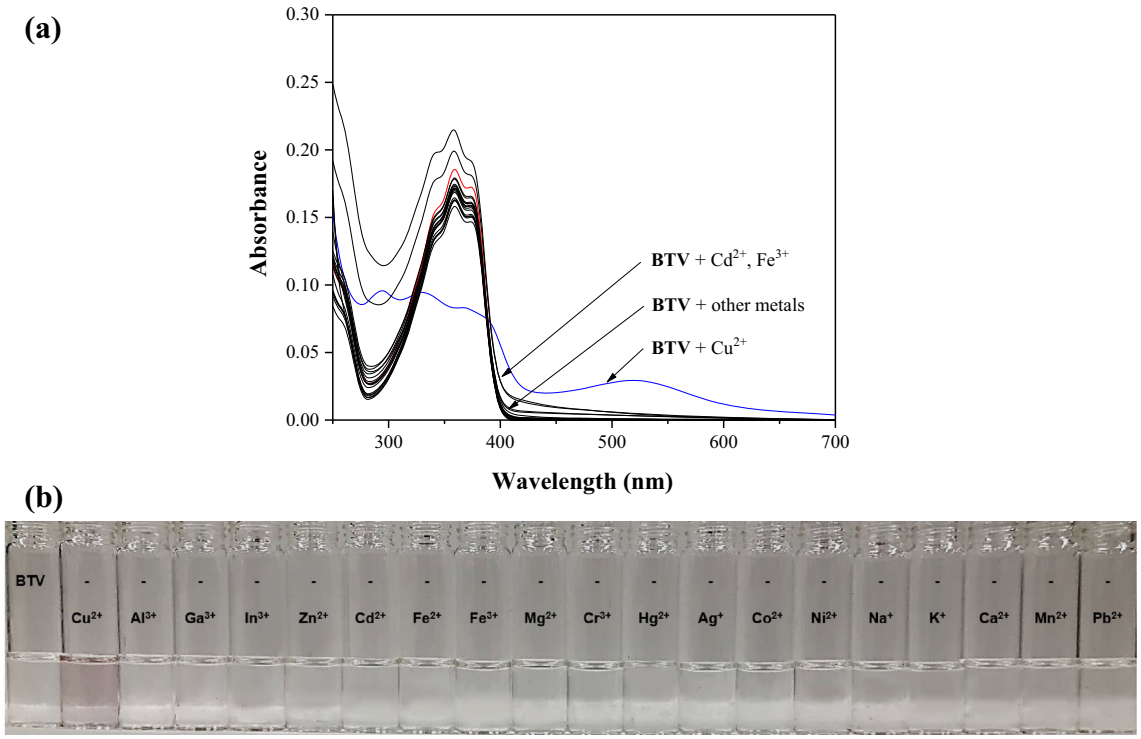

Figure 1. (a) Absorption and (b) colorimetry changes of **BTV** (5×10^{-6} M) with addition of cations (1.6 equiv).

For studying binding properties, the association ratio of **BTV** and Cu^{2+} was determined by Job plot (Figure 4).

The Job plot showed the biggest absorbance, when the ratio of **BTV** and Cu^{2+} was about 0.3.[51] That is, one **BTV** molecule reacted with two Cu^{2+} ions, indicating the 1:2 binding ratio of **BTV** and Cu^{2+}. This result was established by the ESI-MS test (Figure S5, SI). The big intensity of 665.65 (*m/z*) corresponded to [**BTV** + 2·Cu^{2+} + $3NO_3^-$ + MeCN] (calculated *m/z* = 665.94). Association constant of 1×10^{11} M^{-2} for **BTV**-2·Cu^{2+} was given by Li's equation with the calibration curve (Figure S6, SI).[52] FT-IR analysis was performed to investigate the interaction of **BTV** and Cu^{2+} (Figure S7, SI). **BTV** showed bands around 3,000 cm^{-1} and 1,575 cm^{-1} for the O-H and -C=N- functional groups, respectively. Upon binding of Cu^{2+} with **BTV**, the bands shifted to 3,000–3,500 cm^{-1} and 1,541 cm^{-1}. This suggested that the hydroxyl oxygen and the imine nitrogen might be involved in binding to Cu^{2+}. ^1H NMR titrations were applied to figure out the interaction of **BTV** and Cu^{2+} (Figure S8, SI). When Cu^{2+} ion was added to **BTV**, the hydroxyl H_1 proton at 10.8 ppm was shifted to 9.5 ppm. The imine H_6 proton was shifted from 8.5 to 8.4 ppm. In addition, all the aromatic protons were gradually shifted downfield. Then, the methoxy protons H_2 and the methylamine protons H_{11} moved up-field. This outcome signified that the imine nitrogen, the sulfur of the benzothiazole, and the oxygens of the *o*-vanillin would bind to Cu^{2+}. With the analysis of UV-visible titration, ESI-MS, Job plot, FT-IR and ^1H NMR titration, a likely structure of **BTV** with Cu^{2+} was suggested (Scheme 2).

To verify the clear selectivity of **BTV** to Cu^{2+}, the absorbance change of **BTV** with Cu^{2+} was tested with other cations (Figure 5).

BTV had a slight decrease in absorption where Cu^{2+} existed with Al^{3+}, Fe^{2+}, $Cr^{3+,}$ and K^+. However, these changes did not give an influence on the naked eye. Thus, interference of other metals was not shown for sensing Cu^{2+} with **BTV**.

To test the availability of **BTV**, it was applied in colorimetric test strips (Figure 6).

The tests with varying amounts of Cu^{2+} displayed that **BTV** can probe Cu^{2+} through a clear color change to a low concentration of 0.25 mM (Figure 6(a)). In addition, the application of **BTV** to other cations at 0.25 mM demonstrated that copper ion was clearly detected in a paper application (Figure 6(b)). These outcomes illustrated that **BTV**

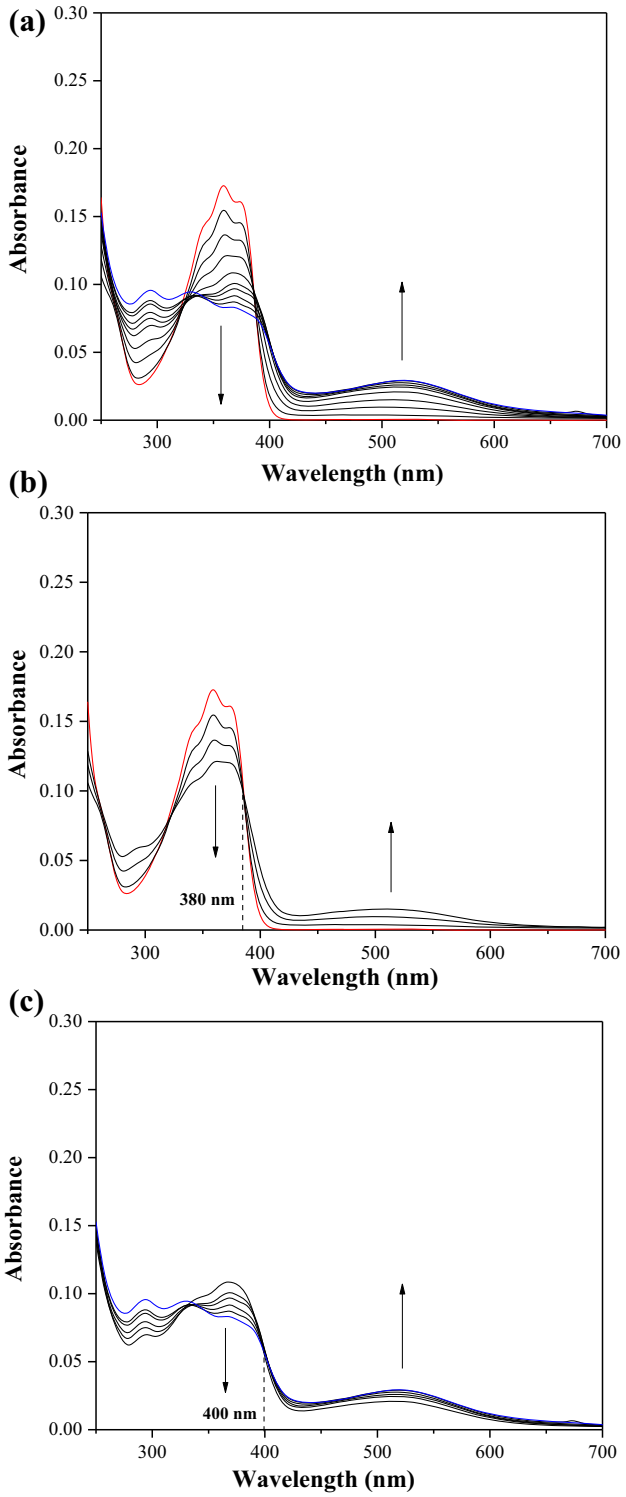

Figure 2. (a) UV-visible spectral change of **BTV** (5×10^{-6} M) at varied Cu^{2+} concentrations (0–1.8 equiv). (b) UV-visible spectral change of **BTV** (5×10^{-6} M) at varied Cu^{2+} concentrations (0–0.6 equiv). (c) UV-visible spectral change of **BTV** (5×10^{-6} M) at different Cu^{2+} concentrations (0.8–1.8 equiv).

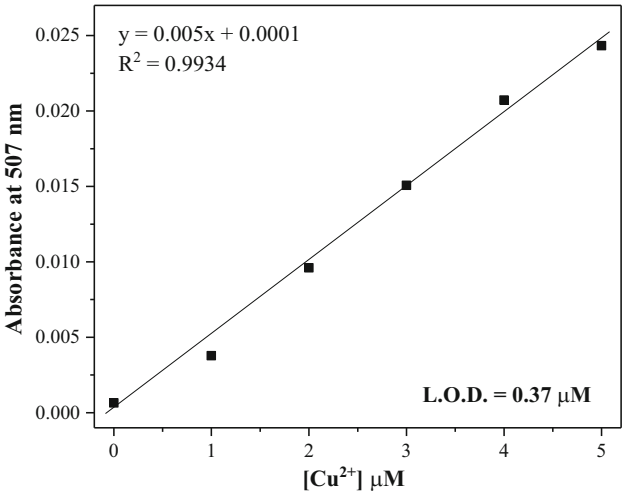

Figure 3. Detection limit of **BTV** to Cu^{2+} using 3σ/slope.

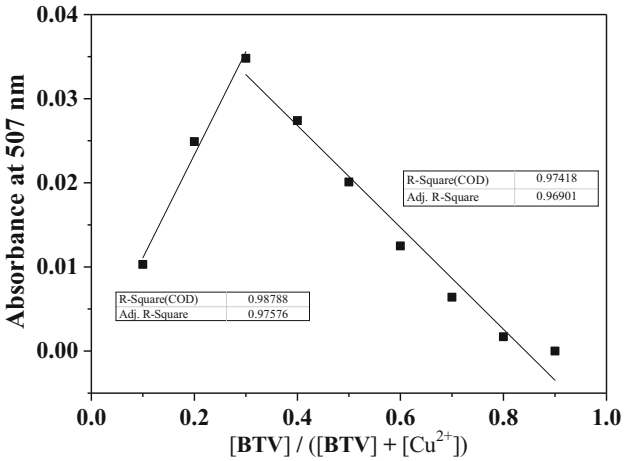

Figure 4. Job plot for **BTV** with Cu^{2+}.

was practically applicable for probing Cu^{2+} using test strips.

3.2 *Calculations of BTV and BTV-2·Cu^{2+}*

Based on Job plot and ESI-MS, the optimized structures of **BTV** and **BTV**-2·Cu^{2+} were calculated (Figure 7).

BTV showed a planer form with dihedral angles of -0.367 ° (1S, 2C, 3N, 4N) and -2.087 ° (5O, 6C, 7C, 8O). The complex state of **BTV** and Cu^{2+} displayed a twisted form with dihedral angles of -13.473 ° (1S, 2C, 3N, 4N) and 1.339 ° (5O, 6C, 7C, 8O).

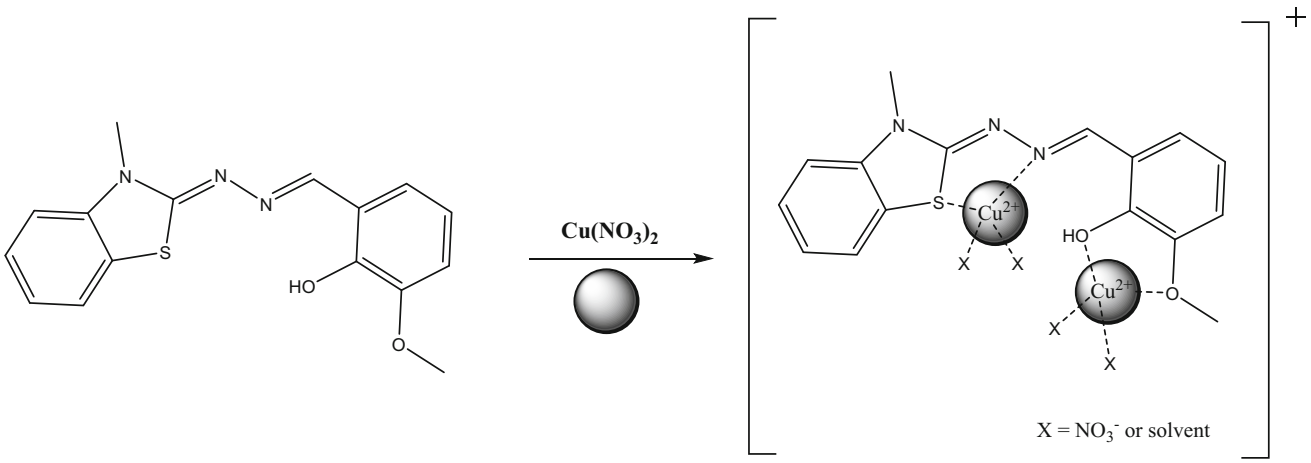

Scheme 2. Plausible structure of **BTV**-2·Cu^{2+}.

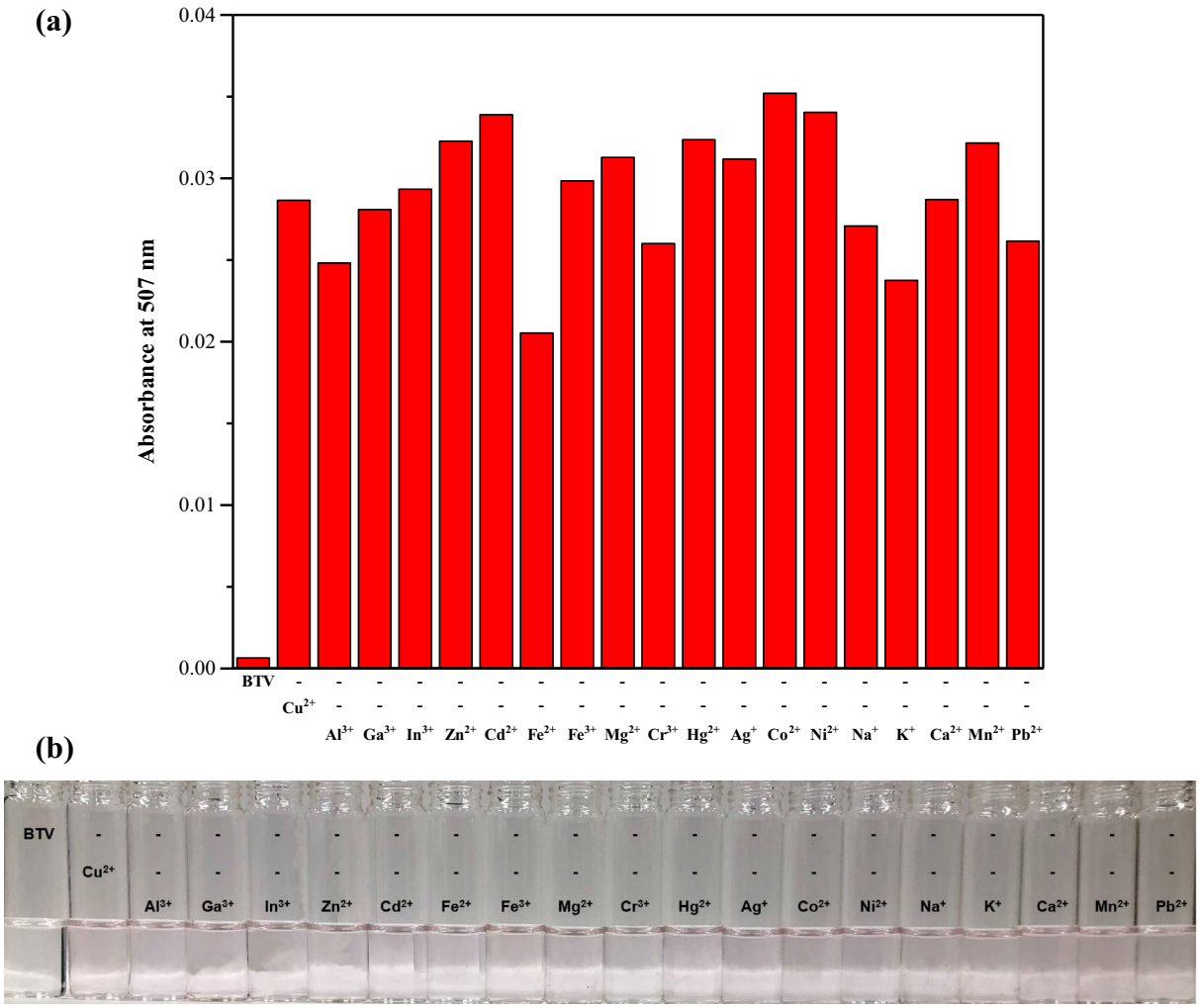

Figure 5. (a) Inhibition test of **BTV** (5×10^{-6} M) upon the addition of Cu^{2+} with other varied metals (1.6 equiv). (b) Photographs of **BTV**, **BTV**-Cu^{2+} and **BTV**-Cu^{2+} with other metal ions.

With the energy-optimized patterns of **BTV** and **BTV**-2·Cu^{2+}, we conducted TD-DFT calculations. **BTV** showed the leading absorption caused by the highest occupied molecular orbital (HOMO) → lowest unoccupied molecular orbital (LUMO) transition (367.88 nm, Figures S9 and S11, SI),

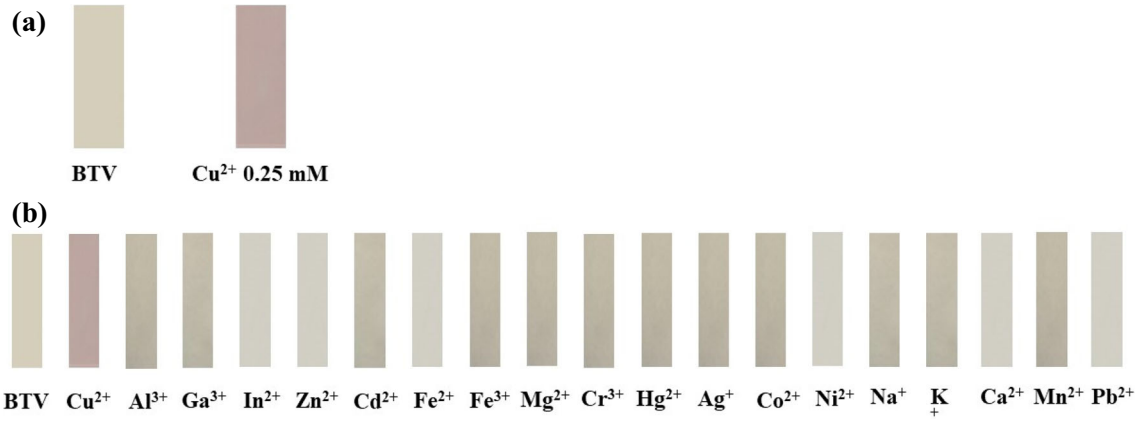

Figure 6. Photographs of the strips stained with **BTV**. (a) **BTV**-strips immersed in 0.25 mM of Cu^{2+}. (b) **BTV**-test strips immersed in varied cations (0.25 mM).

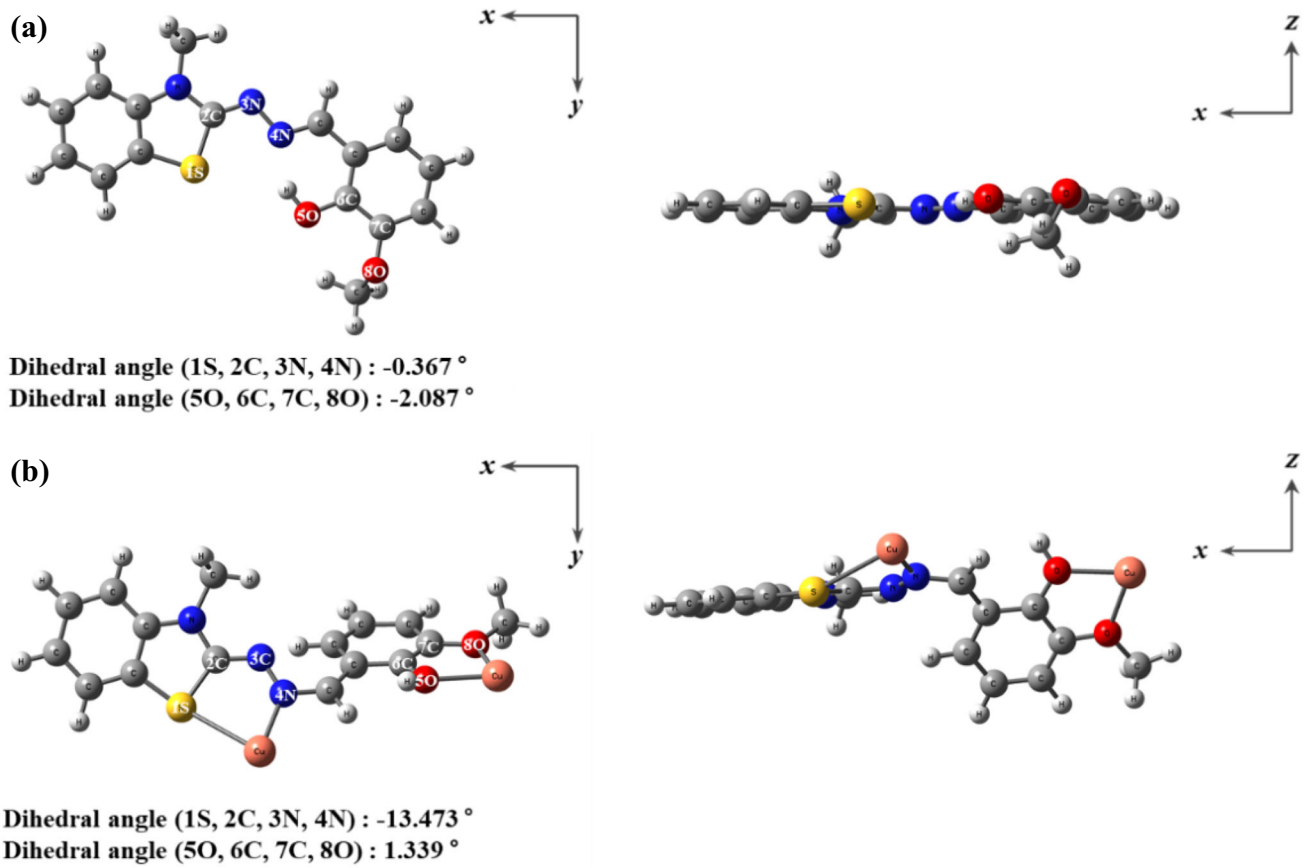

Figure 7. Energy-optimized structures of (a) **BTV** and (b) **BTV**-2·Cu^{2+}.

indicating intramolecular charge transfer (ICT) from the benzothiazole to the *o*-vanillin. **BTV-2**·Cu^{2+} exhibited the major transition at 537.12 nm, induced by the HOMO-7 → LUMO (21%), HOMO-10 → LUMO (39%), HOMO-11 → LUMO (13%), and HOMO-12 → LUMO (13%) (Figures S10 and S11, SI). Except for the HOMO-7 → LUMO transition which showed π → π* transition, transitions at 537.12 nm corresponded to metal-to-ligand charge-transfer (MLCT) characteristic. Thus, MLCT and π → π* transition induce a color variation of **BTV** by binding to Cu^{2+}. In addition, the redshift shown in the experimental spectra was fitted to theoretical results. Referring to the results of the Job plot, calculations, and ESI-MS, we proposed the likely structure of **BTV**-2·Cu^{2+} in Scheme 2.

4. Conclusions

We addressed an efficient benzothiazole-based colorimetry chemosensor **BTV** for detecting Cu^{2+}. **BTV** displayed a color variation from colorless to pink only to Cu^{2+} through bathochromic shift (150 nm). The binding of **BTV** with Cu^{2+} was displayed to be a 1:2, based on ESI-MS and Job plot. The limit of detection for Cu^{2+} with **BTV** was 0.37 μM. Particularly, the value is the lowest among benzothiazole-based colorimetry chemosensors for detecting Cu^{2+}. Then, sensor **BTV** could clearly sense Cu^{2+} without interference from other cations. Distinctly, **BTV** can be used as a test strip by a color variation to detect Cu^{2+}. The detection process of Cu^{2+} by **BTV** was illustrated by the UV-visible, ^{1}H NMR titration, DFT calculation, FT-IR, and ESI-MS.

Supplementary Information (SI)

Experimental procedures and additional experimental data in the form of Tables S1 and Figures S1-S11 can be found at www.ias.ac.in.

Acknowledgements

The National Research Foundation of Korea (2018R1A2B6001686) is gratefully acknowledged.

References

1. Gao X, Yue H, Guo E, Zhang H, Lin X, Yao L and Wang B 2016 Mechanical properties and thermal conductivity of graphene reinforced copper matrix composites *Powder Technol.* **301** 601
2. Lin Q, Chen P, Liu J, Fu Y P, Zhang Y-M and Wei T B 2013 Colorimetric chemosensor and test kit for detection copper(II) cations in aqueous solution with specific selectivity and high sensitivity *Dyes Pigm.* **98** 100
3. Yamamoto R, Kowalski D, Zhu R, Wada K, Sato Y, Kitano S, et al. 2021 Fabrication of superhydrophobic copper metal nanowire surfaces with high thermal conductivity *Appl. Surf. Sci.* **537** 147854
4. Zuo T, Xue J, Ru Y, Gao Z, Zhang L, Da B, et al. 2021 The improved softening resistance and high electrical conductivity of the 3D graphene enhanced copper-based composite fabricated by liquid carbon source *Mater. Lett.* **283** 128895
5. Narayanaswamy N and Govindaraju T 2012 Aldazine-based colorimetric sensors for Cu^{2+} and Fe^{3+} *Sens. Actuat. B Chem.* **161** 304
6. Shrivastava A K 2009 A review on copper pollution and its removal from water bodies by pollution control technologies *Indian J. Environ. Prot.* **29** 552
7. Zhang L, Zhang J, Kuang Q, Xie S, Jiang Z, Xie Z and Zheng L 2011 Cu^{2+}-assisted synthesis of hexoctahedral Au-Pd alloy nanocrystals with high-index facets *J. Am. Chem. Soc.* **133** 17114
8. Liu M, Wang K, Wang H, Lu J, Xu S, Zhao L, et al. 2021 Simple and sensitive colorimetric sensors for the selective detection of Cu(ii) *RSC Adv.* **11** 11732
9. Paisuwan W, Ajavakom V, Sukwattanasinitt M, Tobisu M and Ajavakom A 2022 Ratiometric and colorimetric detection of Cu^{2+} via the oxidation of benzodihydroquinoline derivatives and related synthetic methodology *Sens. Bio-Sens. Res.* **35** 100470
10. Isaad J and Achari A E 2021 Sequential colorimetric sensor for copper(II) and cyanide ions via the complexation-decomplexation mechanism based on sugar pyrazolidine-3,5-dione *J. Mol. Struct.* **1252** 132151
11. Marques D M, Veroneze Júnior V, da Silva A B, Mantovani J R, Magalhães P C and de Souza T C 2018 Copper toxicity on photosynthetic responses and root morphology of *Hymenaea courbaril* L. (Caesalpinioideae) *Water Air Soil Pollut.* **229** 138
12. Chen J, Zhang H, Li J, Liu Y, Shi W and Hu H 2020 The toxic factor of copper should be adjusted during the ecological risk assessment for soil bacterial community *Ecol. Indic.* **111** 106072
13. Goswami S, Sen D and Das N K 2010 A new highly selective, ratiometric and colorimetric fluorescence sensor for Cu^{2+} with a remarkable red shift in absorption and emission spectra based on internal charge transfer *Org. Lett.* **12** 856
14. Wei Z, Wang J, Zhu L, Wang J and Zhu G 2018 Toxicity of enrofloxacin, copper and their interactions on soil microbial populations and ammonia-oxidizing archaea and bacteria *Sci. Rep.* **8** 1
15. Bayindir S and Toprak M 2019 A novel pyrene-based selective colorimetric and ratiometric turn-on sensing for copper *Spectrochim. Acta Part A* **213** 6
16. Jegan A, Pannipara M, Al-Sehemi A G and Phang S M 2020 Synthesis of new Schiff's base copper conjugate for optically and electrochemically tuning of L-cysteine in cancer cells and bovine serum albumin *Sens. Actuat. B Chem.* **316** 128082
17. Mujawar L H, Ismail I M I, Rehan Z A and El-Shahawi M S 2017 A miniaturized assay for sensitive determination of Cu^{2+} ions on nanolitre arrayed 4-(2-pyridylazo)resorcinol (PAR) spots on polyethersulfone membrane platform *J. Mol. Liq.* **229** 574
18. Kim B Y, Pandith A, Cho C S and Kim H-S 2019 Highly selective fluorescent probe based on 2-(2′-dansylamidophenyl)-thiazole for sequential sensing of copper(II) and iodide ions *Bull. Korean Chem. Soc.* **40** 163
19. Sik Na W, Raj P, Singh N and Jang D O 2019 Benzothiazole-based heterodipodal chemosensor for Cu^{2+} and CN^{-} ions in aqueous media *Tetrahedron Lett.* **60** 151075
20. Oliveira P R, Lamy-Mendes A C, Rezende E I P, Mangrich A S, Marcolino Junior L H and Bergamini M F 2015 Electrochemical determination of copper ions in

spirit drinks using carbon paste electrode modified with biochar *Food Chem.* **171** 426
21. Altunay N, Gürkan R and Orhan U 2015 A new ultrasonic-assisted cloud-point-extraction procedure for pre-concentration and determination of ultra-trace levels of copper in selected beverages and foods by flame atomic absorption spectrometry *Food Addit. Contam. Part A* **32** 1475
22. So H, Chae J B and Kim C 2019 A thiol-containing colorimetric chemosensor for relay recognition of Cu^{2+} and S^{2-} in aqueous media with a low detection limit *Inorg. Chim. Acta* **492** 83
23. Maity D and Govindaraju T 2011 Highly selective visible and near-IR sensing of Cu^{2+} based on thiourea-salicylaldehyde coordination in aqueous media *Chem. A Eur. J.* **17** 1410
24. Mahapatra A K, Hazra G, Das N K and Goswami S 2011 A highly selective triphenylamine-based indolylmethane derivatives as colorimetric and turn-off fluorimetric sensor toward Cu^{2+} detection by deprotonation of secondary amines *Sens. Actuat. B Chem.* **156** 456
25. Upadhyay S, Singh A, Sinha R, Omer S and Negi K 2019 Colorimetric chemosensors for d-metal ions: A review in the past, present and future prospect *J. Mol. Struct.* **1193** 89
26. Chan W C, Saad H M, Sim K S, Lee V S, Ang C W, Yeong K Y and Tan K W 2021 A rhodamine based chemosensor for solvent dependent chromogenic sensing of cobalt (II) and copper(II) ions with good selectivity and sensitivity: Synthesis, filter paper test strip, DFT calculations and cytotoxicity *Spectrochim. Acta Part A* **262** 120099
27. Singh N and Chandra R 2021 A naked-eye colorimetric sensor based on chalcone for the sequential recognition of copper(II) and sulfide ions in semi-aqueous solution: Spectroscopic and theoretical approaches *New J. Chem.* **45** 10340
28. Udhayakumari D, Velmathi S, Venkatesan P and Wu S P 2015 Anthracene coupled thiourea as a colorimetric sensor for F^-/Cu^{2+} and fluorescent sensor for Hg^{2+}/picric acid *J. Lumin.* **161** 411
29. Soufeena P P, Nibila T A and Aravindakshan K K 2019 Coumarin based yellow emissive AIEE active probe: A colorimetric sensor for Cu^{2+} and fluorescent sensor for picric acid *Spectrochim. Acta Part A* **223** 117201
30. Cheah P W, Heng M P, Saad H M, Sim K S and Tan K W 2021 Specific detection of Cu^{2+} by a pH-independent colorimetric rhodamine based chemosensor *Opt. Mater. Amst.* **114** 110990
31. Wang Y, Mao P D, Wu W N, Mao J, Zhao L, Xu ZQ, et al. 2017 A novel colorimetric and ratiometric fluorescent Cu^{2+} sensor based on hydrazone bearing 1,8-naphthalimide and pyrrole moieties *Sens. Actuat. B Chem.* **251** 813
32. Jiang H, Li Z, Kang Y, Ding L, Qiao S, Jia S, et al. 2017 A two-photon fluorescent probe for Cu^{2+} based on dansyl moiety and its application in bioimaging *Sens. Actuat. B Chem.* **242** 112
33. Shi F, Cui S, Liu H and Pu S 2020 A high selective fluorescent sensor for Cu^{2+} in solution and test paper strips *Dyes Pigm.* **173** 107914
34. Jung H J, Singh N, Lee D Y and Jang D O 2010 Single sensor for multiple analytes: chromogenic detection of I^- and fluorescent detection of Fe^{3+} *Tetrahedron Lett.* **51** 3962
35. Kaur I, Sharma V, Mobin SM, Khajuria A, Ohri P, Kaur P and Singh K 2019 Aggregation tailored emission of a benzothiazole based derivative: Photostable turn on bioimaging *RSC Adv.* **9** 39970
36. Zhang S, Wu X, Niu Q, Guo Z, Li T and Liu H 2017 Highly selective and sensitive colorimetric and fluorescent chemosensor for rapid detection of Ag^+, Cu^{2+} and Hg^{2+} based on a simple Schiff base *J. Fluoresc.* **27** 729
37. Weng J, Mei Q, Zhang B, Jiang Y, Tong B, Fan Q, et al. 2013 Multi-functional fluorescent probe for Hg^{2+}, Cu^{2+} and ClO^- based on a pyrimidin-4-yl phenothiazine derivative *Analyst* **138** 6607
38. Na Y J, Choi Y W, Yun J Y, Park K M, Chang P S and Kim C 2015 Dual-channel detection of Cu^{2+} and F^- with a simple Schiff-based colorimetric and fluorescent sensor *Spectrochim. Acta Part A* **136** 1649
39. Frisch M J, Trucks G W, Schlegel H B, Scuseria G E, Robb M A, Cheeseman J R, Scalmani G, Barone V, Mennucci B, Petersson G A, Nakatsuji H, Caricato M, Li X, Hratchian H P, Izmaylov A F, Bloino J, Zheng G, Sonnenberg J L, Had M 2009. G09 | Gaussian.com.
40. Becke A D 1993 Density-functional thermochemistry. III. The role of exact exchange *J. Chem. Phys.* **98** 5648
41. Lee C, Yang W and Parr R G 1988 Development of the Colle-Salvetti correlation-energy formula into a functional of the electron density *Phys. Rev. B* **37** 785
42. Hay P J and Wadt W R 1985 Ab initio effective core potentials for molecular calculations. Potentials for the transition metal atoms Sc to Hg *J. Chem. Phys.* **82** 270
43. Wadt W R and Hay P J 1985 Ab initio effective core potentials for molecular calculations. Potentials for main group elements Na to Bi *J. Chem. Phys.* **82** 284
44. Hariharan P C and Pople J A 1973 The influence of polarization functions on molecular orbital hydrogenation energies *Theor. Chim. Acta* **28** 213
45. Francl M M, Pietro W J, Hehre W J, Binkley J S, Gordon M S, DeFrees D J and Pople J A 1982 Selfconsistent molecular orbital methods. XXIII. A polarizationtype basis set for secondrow elements *J. Chem. Phys.* **77** 3654
46. Klamt A, Moya C and Palomar J 2015 A comprehensive comparison of the IEFPCM and SS(V)PE continuum solvation methods with the COSMO approach *J. Chem. Theor. Comput.* **11** 4220
47. Tang L, Dai X, Wen X, Wu D and Zhang Q 2015 A rhodamine-benzothiazole conjugated sensor for colorimetric, ratiometric and sequential recognition of copper(II) and sulfide in aqueous media *Spectrochim. Acta Part A* **139** 329
48. Ghosh K and Kar D 2013 Anthraquinone coupled benzothiazole-based receptor for selective sensing of Cu^{2+} *J. Incl. Phenom. Macrocycl. Chem.* **77** 67

49. Cao X, Gao Q, He X, Bai Y and Sun W 2020 A colorimetric probe for detection of Cu^{2+} by the naked eye and application in test paper *Luminescence* **35** 651
50. Suh B, Choe D and Kim C 2021 An effective colorimetric sensor for detecting Cu^{2+} based on benzothiazole moiety *Color Technol.* **137** 512
51. Renny J S, Tomasevich L L, Tallmadge E H and Collum D B 2013 Method of continuous variations: Applications of job plots to the study of molecular associations in organometallic chemistry *Angew. Chem. Int. Ed.* **52** 11998
52. Grynkiewicz G, Poenie M and Tsien R Y 1985 A new generation of Ca^{2+} indicators with greatly improved fluorescence properties *J. Biol. Chem.* **260** 3440